Calycosin attenuates diabetic vascular injury through anti-glycation, anti-inflammatory and endothelial metabolic effects

JUNFENG SHI[1,2*], HUIRU TANG[1,2*], JIAN CHEN[3*], WEIXIU QIU[1,2], YINGJIE WANG[1,2], WANQIU ZHANG[1,2], CHENGXIA KAN[1,2], YUJIE MA[2], HONGYAN QIU[1,2] and XIAODONG SUN[1,2]

[1]Department of Endocrinology and Metabolism, Affiliated Hospital of Shandong Second Medical University, School of Clinical Medicine, Shandong Second Medical University, Weifang, Shandong 261031, P.R. China; [2]Shandong Provincial Key Medical and Health Laboratory for Endocrinology and Metabolic Diseases, Clinical Research Center, Affiliated Hospital of Shandong Second Medical University, Weifang, Shandong 261031, P.R. China; [3]Guangxi Key Laboratory of Tumor Immunology and Microenvironmental Regulation, Guilin Medical University, Guilin, Guangxi 541001, P.R. China

Received July 21, 2026; Accepted November 6, 2026

DOI: 10.3892/ijmm.2026.6060

Abstract. Advanced glycation end-products (AGEs) contribute to diabetes-associated endothelial injury; however, there are a limited number of therapies that target glycation-associated inflammation and endothelial metabolic abnormalities. Calycosin is a bioactive isoflavone with anti-inflammatory and antioxidant properties; however, its vascular protective effects in diabetes have not yet been well characterized. In the present study, AGE-treated human umbilical vein endothelial cells (HUVECs) and mice with high-fat diet/streptozotocin-induced diabetes were used to investigate the effects of calycosin. Endothelial viability, apoptosis, nitric oxide (NO) release and RAGE/NF-κB signaling were examined, and untargeted metabolomic and proteomic analyses were performed. Vascular histopathology, permeability, vasorelaxation, plasma AGE-associated fluorescence, albumin glycation, blood glucose concentration and glucose tolerance were evaluated *in vivo*. Calycosin attenuated the AGE-induced reductions in HUVEC viability and NO release, as well as the increases in apoptosis, RAGE expression and NF-κB phosphorylation. Untargeted metabolomics identified 725 metabolites and revealed an amelioration of the AGE-induced metabolic defects, particularly in lipid and amino acid metabolism. Proteomic analysis identified changes in the expression of RAGE-associated signaling proteins, including protein diaphanous homolog 1 (DIAPH1), transcription factor p65 (RELA) and urokinase-type plasminogen activator (PLAU). Pharmacological inhibition of RAGE with FPS-ZM1 attenuated AGE-induced NF-κB phosphorylation. In diabetic mice, calycosin reduced the plasma AGE-associated fluorescence and glycation of albumin, alleviated vascular remodeling and inflammation, reduced vascular permeability, and improved acetylcholine-induced vasorelaxation. Calycosin also reduced the blood glucose concentrations and improved the glucose tolerance of the mice. Collectively, these findings indicate that calycosin attenuates diabetic vascular injury, reduces glycation and proinflammatory signaling, and modulates endothelial metabolism. These data support the potential use of calycosin as a candidate therapy for the vascular complications of diabetes.

Introduction

Diabetes mellitus is a chronic metabolic disorder characterized by sustained hyperglycemia and progressive systemic complications. Its increasing global prevalence poses a major public health challenge (1). Cardiovascular disease remains a leading cause of morbidity and mortality for patients with diabetes, and endothelial dysfunction is an early defect in the development of the vascular complications of diabetes. Therefore, therapies aimed at preserving endothelial integrity and vascular function would be of great interest (2).

Advanced glycation end-products (AGEs) are key mediators of the effects of chronic hyperglycemia on the vasculature. The non-enzymatic glycation of circulating and tissue proteins promotes the accumulation of AGEs under diabetic conditions. AGEs interact with the receptor for advanced glycation end-products (RAGE), thereby activating multiple downstream pathways, including the MAPK/ERK, JAK/STAT, PI3K/Akt, NF-κB and NADPH oxidase/reactive oxygen species pathways (3). These responses promote oxidative stress and inflammation, reduce endothelial nitric oxide (NO) bioavailability, increase vascular permeability and contribute

Correspondence to: Dr Xiaodong Sun or Dr Hongyan Qiu, Department of Endocrinology and Metabolism, Affiliated Hospital of Shandong Second Medical University, School of Clinical Medicine, Shandong Second Medical University, 2428 Yuhe Road, Weifang, Shandong 261031, P.R. China
Email: xiaodong.sun@sdsmu.edu.cn
E-mail: qiuhongyan@sdsmu.edu.cn

*Contributed equally

Key words: calycosin, advanced glycation end-product, endothelial dysfunction, RAGE/NF-κB signaling, diabetic vascular complication, metabolomics

to vascular remodeling, thereby causing the progression of diabetic vascular dysfunction (4).

Certain natural, plant-derived substances represent potential therapies for diabetic vascular injury due to their anti-inflammatory, antioxidant and metabolic regulatory properties (5,6). Calycosin, a natural isoflavone that is principally obtained from leguminous plants, has been shown to exert anti-inflammatory, antioxidant, anti-apoptotic and immunomodulatory effects (7-9). Previous studies have shown that calycosin exerts protective effects against several complications of diabetes, including diabetic nephropathy, peripheral neuropathy and cognitive impairment, as well as gestational diabetes. These effects are associated with the attenuation of AGE/RAGE and NF-κB-related proinflammatory signaling, a reduction in oxidative stress and the regulation of metabolic signaling pathways, such as the AMPK/SKP2/CARM1 pathway (10-17). These findings highlight the potential for the use of calycosin in the management of the complications of diabetes.

The vascular protective effects of calycosin in diabetes have not yet been well characterized. In particular, its effects on systemic glycation, RAGE-associated inflammatory signaling and endothelial metabolic remodeling have not been systematically investigated. Therefore, the present study used AGE-treated human umbilical vein endothelial cells (HUVECs) and mice with high-fat diet/streptozotocin (STZ)-induced diabetes to evaluate the vascular protective effects of calycosin. Using endothelial metabolomic and proteomic profiling, plasma AGE measurements, albumin glycation-site analysis, vascular histopathology, permeability measurements and *ex vivo* vasorelaxation assays, the present study aimed to characterize the protective effects of calycosin against diabetic vascular injury and the associated molecular alterations.

Materials and methods

Preparation of AGEs. AGEs were prepared by incubating 35 mg/ml human serum albumin (HSA; MilliporeSigma) with 0.5 M glucose in phosphate-buffered saline (PBS; Wuhan Servicebio Technology Co., Ltd.) at 37˚C for 3 months. The resulting solution was repeatedly ultra-filtered using a 30-kDa molecular weight cut-off membrane to remove free glucose and other low-molecular-weight components. The protein concentration and AGE content of this preparation were determined using a BCA assay (Thermo Fisher Scientific, Inc.) and an AGE assay kit (Abcam), respectively. The AGE-modified HSA was then lyophilized for use in subsequent experiments. For the non-glycated albumin control, HSA was prepared under identical conditions, but without the addition of glucose. This preparation was then used at the same protein concentration as that of the AGE-modified HSA in subsequent experiments performed using HUVECs.

Cells, cell culture and maintenance, and the RAGE inhibition assay. Immortalized HUVECs (PUMC-HUVEC-T1, cat. no. FH1199; Shanghai Fuheng Biotechnology Co., Ltd.) were maintained in DMEM (Wuhan Servicebio Technology Co., Ltd.) supplemented with 10% fetal bovine serum (Vivacell) and 1% penicillin/streptomycin (Wuhan Servicebio Technology Co., Ltd.) at 37˚C. For all the experiments, the cells were used between passages 5 and 15, when they had reached 80-90% confluency.

For the *in vitro* experiments, the cells were assigned to the following groups: A normal culture medium (CT group), a medium supplemented with 800 μg/ml AGEs (AGE group), and a medium containing both 800 μg/ml AGEs and 10 μM calycosin (Chengdu Must Bio-Technology Co., Ltd.; calycosin group). Calycosin was dissolved in 0.1% dimethyl sulfoxide (DMSO, Beijing Solarbio Science & Technology Co., Ltd.) and an equal amount of DMSO was added to cells in the CT and AGE groups. To inhibit RAGE, the HUVECs were pre-treated with 10 μM FPS-ZM1 (MedChemExpress) for 1 h at 37˚C prior to AGE exposure. DMSO was used as the vehicle control.

Assessment of cell viability, proliferation, nitric oxide release and apoptosis. Cells were seeded at equal densities and subsequently exposed to one of the three treatments for 24 h. Cell viability was assessed using a CCK-8 assay (Wuhan Servicebio Technology Co., Ltd.). Cells were seeded in 96-well plates (5,000 cells/well), treated as indicated, and incubated with 10 μl of CCK-8 reagent at 37˚C for 1 h. Absorbance was measured at 450 nm using a Multiskan FC microplate reader (Thermo Fisher Scientific, Inc.). Images of cells in each group were captured under an inverted phase-contrast microscope (Olympus Corporation). Cell suspensions were mixed 1:1 with 0.2% Trypan blue (Beijing Solarbio Science & Technology Co., Ltd.) at room temperature, without fixation, and immediately analyzed using a Countstar IC1000 automated cell counter (Shanghai Ruiyu Biotech Co., Ltd.). The NO concentrations in the supernatants were determined using a commercial detection kit (Beyotime Biotechnology), absorbance readings and a standard curve. Apoptosis was assessed using Annexin V-FITC (Shanghai Yeasen Biotechnology Co., Ltd.) and flow cytometry (DxFLEX; Beckman Coulter, Inc.).

Immunofluorescence staining. HUVECs were seeded on coverslips in 24-well plates ($5x10^4$ cells/well) and treated with control medium, AGEs, or AGEs plus calycosin for 24 h. The cells were then fixed in 4% paraformaldehyde (Biosharp Life Sciences) for 10 min at room temperature, permeabilized with 0.2% Triton X-100 (Beijing Solarbio Science & Technology Co., Ltd.) for 5 min, and blocked with 5% BSA (Beijing Solarbio Science & Technology Co., Ltd.) for 30 min. Following PBS washes, the cells were incubated with anti-RAGE primary antibody (1:100; cat. no. ab216329, Abcam) overnight at 4˚C, followed by Alexa Fluor 488-conjugated secondary antibody (1:500; cat. no. ab150073, Abcam) for 1 h and DAPI staining solution (C0065, Beijing Solarbio Science & Technology Co., Ltd.) for 2 min at room temperature in the dark. Images were acquired using an imaging system (Thermo Fisher Scientific, Inc.).

Western blot analysis. HUVECs were lysed in RIPA buffer (Beijing Solarbio Science & Technology Co., Ltd.) supplemented with 1% protease inhibitor cocktail and 1% phosphatase inhibitor cocktail. Protein concentrations were determined using a BCA protein assay kit (Wuhan Servicebio Technology Co., Ltd.). The lysates were subsequently mixed with SDS-PAGE loading buffer containing 2% SDS and incubated at room temperature for 30 min for protein denaturation.

For each target protein, equal amounts of protein (30 μg per lane) were loaded across all experimental groups. Proteins were separated by SDS-PAGE and transferred onto polyvinylidene difluoride membranes (Millipore). The membranes were blocked with 5% non-fat milk or, for phosphorylated proteins, 5% BSA at room temperature for 2 h and subsequently incubated overnight at 4˚C with primary antibodies against RAGE (1:1,000; cat. no. ab216329, Abcam), NF-κB (1:1,000; cat. no. 8242S, Cell Signaling Technology, Inc.), p-NF-κB (1:1,000; cat. no. R013789, Epizyme Biotech), or GAPDH (1:50,000; cat. no. 60004-1-Ig, Proteintech Group, Inc.). The membranes were then incubated with the appropriate HRP-conjugated goat anti-rabbit IgG (1:1,000; cat. no. A0208, Beyotime Biotechnology) or goat anti-mouse IgG (1:1,000; cat. no. A0216; Beyotime Biotechnology) for 1 h at room temperature. Protein bands were visualized using an ECL substrate (Shanghai Yanxi Biotechnology Co., Ltd.) and a V3 imaging system (Bio-Rad Laboratories, Inc.). Densitometric analysis was performed using Image Lab software (version 6.1.0, build 7; Bio-Rad Laboratories, Inc.).

Untargeted cell metabolomics. Metabolites were extracted from 2x10^6 HUVECs using 1 ml of precooled 80% methanol (Thermo Fisher Scientific, Inc.). Following sonication and centrifugation (1,000 x g at room temperature for 5 min), the supernatants were vacuum-dried and reconstituted in 50% methanol. LC-MS/MS analysis was performed using a QE Plus mass spectrometer (Thermo Fisher Scientific, Inc.) in positive and negative electrospray ionization modes. The mobile phases consisted of 0.1% formic acid in water (A) and methanol (B), with a flow rate of 0.3 ml/min, and gradient elution was performed. The MS parameters were as follows: Spray voltages, 3.5 kV (positive) and ~2.8 kV (negative); sheath and auxiliary gas settings, 40 and 10, respectively; heater temperature, 350˚C; capillary temperature, 325˚C; scan range, 70-1,000 m/z; resolution, 70,000; column temperature, 35˚C; and injection volume, 5 μl. Metabolites were identified using Compound Discoverer 3.0 (Thermo Fisher Scientific, Inc.). Metabolites present at various concentrations in the three groups were identified and KEGG pathway enrichment analysis was performed using R software (version 4.4.3) and MetaboAnalyst 6.0, using thresholds of FC >1.3 and P<0.05. Quality control (QC) samples were prepared by pooling equally sized aliquots of biological samples, and these were analyzed periodically to confirm the stability of the measurements. The peak areas obtained were normalized, and metabolites for which there were large numbers of missing values or poor QC reproducibility were excluded from the downstream analysis.

Animals and experimental model. A total of 28 male C57BL/6 mice (6 weeks old; weighing ~20 g) were purchased from Jinan Pengyue Experimental Animal Breeding Co., Ltd. Male mice were used as the high-fat diet/STZ model produces a more consistent diabetic phenotype in male than in female C57BL/6 mice. All the animal procedures were performed in compliance with the ARRIVE guidelines and were approved by the Institutional Animal Care and Use Committee of Shandong Second Medical University (approval no. 2024SDL751). The mice were housed under specific pathogen-free conditions at 22±2˚C and 50±10% relative humidity under a 12-h light/dark cycle, with free access to food and water. Following a 3-day acclimatization period, the mice were randomly assigned to the normal control (NC; n=8), diabetes mellitus (DM; n=10), and calycosin treatment (n=10) groups. The DM and calycosin groups were fed a high-fat diet (20/60/20% kcal from proteins/fats/carbohydrates; 5,240 kcal/kg; Wuxi Fanbo Biotechnology Co., Ltd.) for 4 weeks, then intraperitoneally (i.p.) administered 50 mg/kg STZ (MilliporeSigma) daily for 4 days. The high-fat diet/STZ model was selected as this involves both diet-induced metabolic stress and STZ-induced β-cell dysfunction, which is characterized by sustained hyperglycemia, thereby providing a relevant model for the study of the vascular complications of diabetes (18,19). STZ was freshly prepared in citrate buffer (0.1 M citric acid/0.1 M sodium citrate, 1:1, pH 4.5; Shanghai Aladdin Biochemical Technology Co., Ltd.). The presence of diabetes was confirmed when random glucose concentrations >11.1 mmol/l were obtained 1 week following the final STZ injection. Following the successful induction of diabetes, the mice in the calycosin group were i.p. injected with 20 mg/kg calycosin (Chengdu Must Bio-Technology Co., Ltd.) daily for 45 days, and those in the NC and DM groups were injected with equal volumes of saline. During the treatment period, the body masses, blood glucose concentrations, and food and water intakes of the mice were monitored. Oral glucose tolerance testing was performed before and after calycosin treatment, as previously described (20). At the experimental endpoint, mice were deeply anesthetized with 3-4% isoflurane and euthanized by cervical dislocation. Death was confirmed by the absence of respiration and heartbeat. Thoracic aortas and blood samples were then collected for subsequent analyses.

Identification of non-enzymatic glycation sites in plasma albumin. Globulins were removed from mouse plasma samples by PEG-6000 precipitation [Sangon Biotech (Shanghai) Co., Ltd.], and the albumin-containing supernatants were collected. The proteins in the supernatants were denatured using 8 M SDC-urea (MilliporeSigma), their overall concentrations were quantified using a BCA assay (Thermo Fisher Scientific, Inc.), and 200 μg protein per sample were then reduced using 8 mM dithiothreitol (DTT; MilliporeSigma) and alkylated using 16 mM iodoacetamide (IAA; MilliporeSigma). The samples were then digested using trypsin (1:25; Promega Corporation) at 37˚C for 36 h. Following the desalting of 20 μg of the peptides obtained, 600 ng was loaded onto a C18 column (Acclaim PepMap RSLC, 2 μm, 75 μm x250 mm) for nanoLC-MS/MS analysis using the QE Plus mass spectrometer (Thermo Fisher Scientific, Inc.). The peptides were identified using Proteome Discoverer software (version 3.3; Thermo Fisher Scientific, Inc.), and the relative glycation level was determined using the peak areas corresponding to glycated peptides.

Histological and immunohistochemical staining. Blood vessels from the mice were fixed in 4% paraformaldehyde (Biosharp, Beijing Labgic Technology Co., Ltd.) at room temperature for 48 h, paraffin-embedded and sectioned at a thickness of 4 μm. Following deparaffinization and rehydration, the sections were stained using hematoxylin and eosin (H&E; G1076), Masson's trichrome (G1006), or modified Sirius Red (G1078) kits (all from Wuhan Servicebio Technology

Co., Ltd.). H&E staining comprised hematoxylin staining for 3 min and eosin staining for 15 sec at room temperature. Masson's staining comprised 2.5% potassium dichromate treatment at 65˚C for 30 min, followed at room temperature by Weigert's iron hematoxylin (1 min), Ponceau-acid fuchsin (6 min), 1% phosphomolybdic acid (1 min) and 2.5% aniline blue (2-30 sec). Sirius Red staining comprised mordanting at 65˚C for 30 min, differentiation for 2 min, and staining for 1 h at room temperature. For immunohistochemistry, the sections were incubated with anti-NF-κB primary antibody (1:1,000; cat. no. 8242S, Cell Signaling Technology, Inc.) overnight at 4˚C, then with an HRP-conjugated secondary antibody (GB23303; Wuhan Servicebio Technology Co., Ltd.; 1:500) for 1 h at room temperature, with DAB being used for chromogenic detection. Finally, the sections were counterstained with hematoxylin (Wuhan Servicebio Technology Co., Ltd.) and mounted. Images were acquired using an EVOS M7000 system (Thermo Fisher Scientific, Inc.) at x200 magnification and quantified using ImageJ software (version 1.46r; National Institutes of Health).

Fluorometric assay of plasma AGEs. Plasma samples from the mice were collected in anticoagulant-containing tubes, then centrifuged (1,500-2,000 x g, 4˚C, 15 min), and the resultant supernatant was assayed for AGE-specific fluorescence (Ex/Em wavelengths 355/460 nm) using a multimode microplate reader (Flash, SuPerMax 3100; Shanghai Shanpu Biotechnology Co., Ltd.).

Evans blue permeability assay. Mice were injected with 2% Evans blue solution (4 μl/g, Beijing Solarbio Science & Technology Co., Ltd.) via a tail vein, then 1 h later, they were perfused with cold 0.9% NaCl through their left ventricles. Their thoracic aortas were collected, rinsed, embedded in OCT compound and frozen on dry ice. Frozen sections (thickness of 7 μm) were prepared at -20˚C and then examined using the red fluorescence channel of the EVOS M7000 imaging system (Thermo Fisher Scientific, Inc.).

Vasodilation assay. Thoracic aortas were cut into 4-6-mm-long rings and mounted in Krebs-Henseleit buffer at 37˚C (95% O_2/5% CO_2) under a resting tension of 1 g. Following 60 min of equilibration, with buffer replacement every 15-20 min, vascular viability was confirmed using 60 mM KCl (Shanghai Macklin Biochemical Co., Ltd.). The rings were then precontracted using norepinephrine (NE; 1 μM; Shanghai Yingxin Laboratory Equipment Co., Ltd.) treatment and subsequently exposed to increasing concentrations of acetylcholine (ACh; 10^{-8}-10^{-4} M; MilliporeSigma). Changes in tension were then recorded using a force transducer and data acquisition system (ADInstruments).

Cellular proteomics. Cells were lysed in SDC-urea buffer (MilliporeSigma) and then sonicated (250 W, 1 min; 3 sec on/7 sec off). Following centrifugation (13,000 x g at 4˚C for 15 min), samples containing 100 μg protein were reduced using 20 mM DTT at 56˚C for 20 min, then alkylated using 40 mM IAA for 30 min in the dark. The proteins were precipitated using 10% trichloroacetic acid solution (MilliporeSigma) at -20˚C for 2 h, washed with ice-cold acetone, vacuum-dried and digested with trypsin (1:25, w/w; Promega Corporation) at 37˚C for 36 h. The peptides were then reconstituted in 0.1% formic acid (FA)/2% acetonitrile (ACN) and analyzed using a Vanquish Neo UHPLC system coupled to an Orbitrap Astral mass spectrometer (Thermo Fisher Scientific, Inc.). The mobile phases consisted of 0.1% formic acid in water (A) and 0.1% formic acid in 80% acetonitrile (B). All mobile-phase reagents were obtained from Thermo Fisher Scientific, Inc. The peptides were separated using an Easy-spray analytical column (150 μm x 150 mm, 2 μm, 100 Å; Thermo Fisher Scientific, Inc.) following trap-column loading.

Statistical analysis. The data are presented as the mean ± standard deviation (SD). Statistical analyses were performed using GraphPad Prism 9.0 or R 4.4.3. The groups were compared using one-way ANOVA with Tukey's multiple-comparisons test. Longitudinal data and concentration-response curves were analyzed using two-way repeated-measures ANOVA followed by Sidak post hoc tests. Metabolites present at different concentrations in the groups were identified using a fold-difference threshold of >1.3 and $P<0.05$, and these were then subjected to KEGG pathway enrichment analysis. A value of $P<0.05$ was considered to indicate a statistically significant difference.

Results

Calycosin preserves endothelial viability and function in AGE-exposed HUVECs. HUVECs were exposed to 800 μg/ml AGEs to induce endothelial injury. Exposure to AGEs significantly reduced cell viability vs. the control group (CT: 100.3% vs. AGE: 81.2%; $P<0.0001$); however, treatment with 10 μM calycosin restored cell viability to 103.5% ($P<0.0001$; Fig. 1A). Consistent with this, calycosin partially reversed the AGE-induced reduction in cell number (Fig. 1B). Annexin V-FITC/PI staining revealed that calycosin reduced AGE-induced apoptosis (CT: 13.0%; AGE: 26.4%; calycosin: 16.5%; $P<0.01$; Fig. 1C-F). The morphological abnormalities induced by AGEs were also reduced by treatment with calycosin (Fig. 1G). Furthermore, exposure to AGEs significantly reduced NO release (CT: 0.5 μM vs. AGE: 0.3 μM; $P<0.0001$); however, calycosin increased the NO level to 0.4 μM ($P=0.0049$; Fig. 1H). These findings indicate that calycosin attenuates AGE-induced endothelial injury by preserving cell viability, reducing apoptosis and increasing NO release. Of note, when non-glycated HSA was used as a control, there were no significant differences in the cell viability, cell number or NO release vs. the CT group ($P>0.05$), and no apparent morphological differences. By contrast, AGE-modified HSA significantly affected these parameters and induced morphological abnormalities (Fig. S1). These findings suggest that the endothelial injury was primarily associated with the glycation of albumin, rather than albumin exposure alone.

Calycosin attenuates the AGE-induced upregulation of the RAGE/NF-κB pathway in HUVECs. The present study then examined the effects of calycosin on AGE/RAGE-associated pro-inflammatory signaling. Immunofluorescence staining demonstrated that exposure to AGEs significantly increased the RAGE-associated fluorescence intensity vs. the control

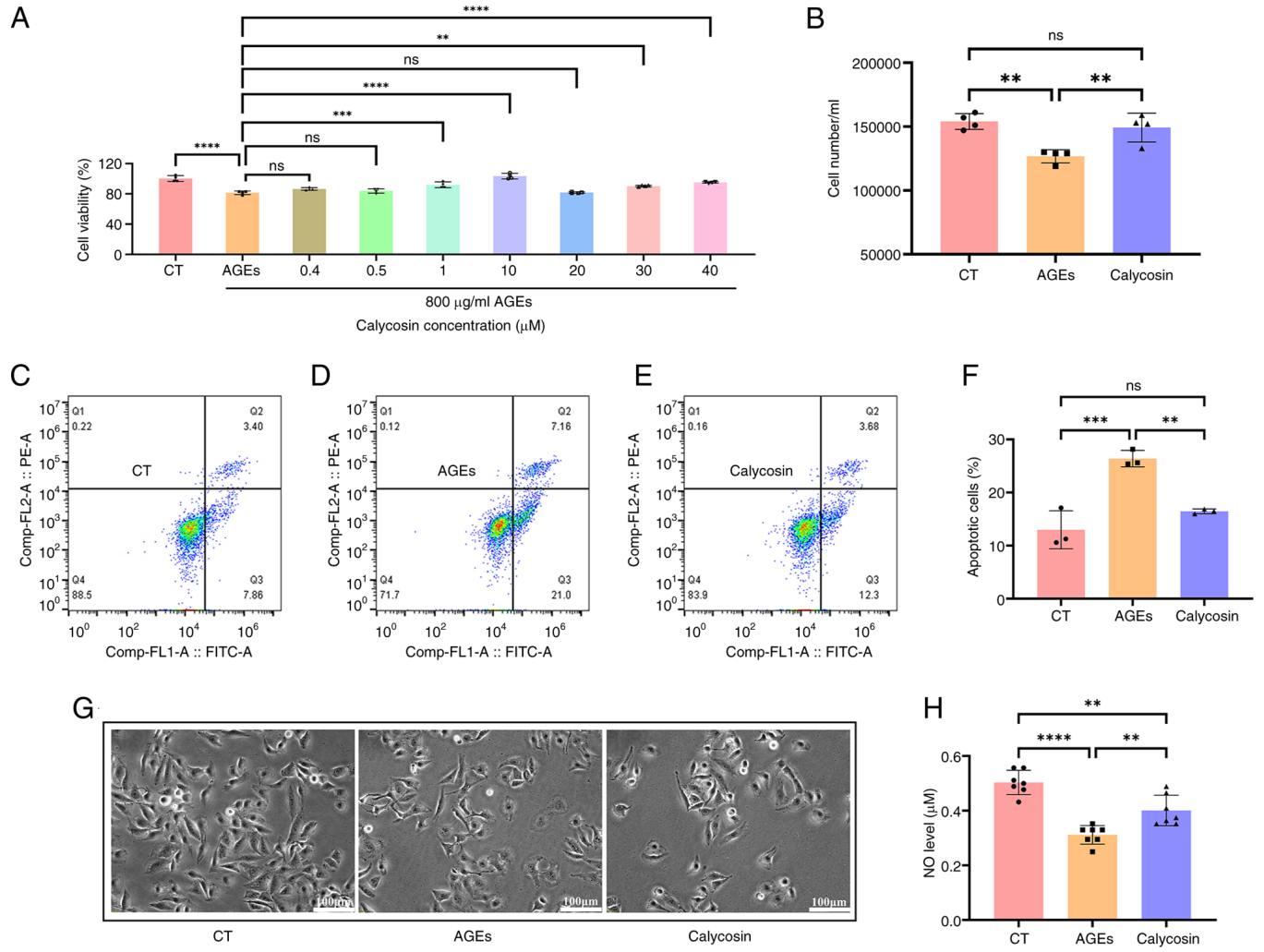


Figure 1. Calycosin preserves endothelial viability and function in human umbilical vein endothelial cells exposed to AGEs. (A) CCK-8 assay of cell viability (n=4). (B) Cell number (n=4). (C-F) Representative flow cytometry plots and quantification of apoptosis (n=3). (G) Representative morphological images (magnification, x20). (H) NO release (n=7). AGEs, advanced glycation end-products; NO, nitric oxide; CT, normal culture medium; ns, not significant; **P<0.01; ***P<0.001; ****P<0.0001.

cells (P<0.0001); however, calycosin attenuated this increase (P<0.001; Fig. 2A and B). Western blot analysis revealed that exposure to AGEs increased the expression of the RAGE protein (P<0.05) and NF-κB phosphorylation (P<0.01), whereas both of these defects were significantly ameliorated by calycosin (P<0.05; Fig. 2C-E). These findings suggest that the endothelial protective effect of calycosin is associated with the attenuation of RAGE/NF-κB pro-inflammatory signaling. To further assess the involvement of RAGE, HUVECs were treated with the RAGE antagonist, FPS-ZM1, prior to their exposure to AGEs. FPS-ZM1 significantly reduced the phosphorylation of NF-κB (P<0.01) and the p-NF-κB/NF-κB ratio (P<0.05), without significantly altering total NF-κB expression (Fig. S2). These results provide pharmacological evidence that RAGE contributes to the AGE-induced activation of NF-κB.

Calycosin ameliorates the AGE-induced changes in endothelial metabolism. The untargeted LC-MS/MS metabolomic analysis identified 725 metabolites in the HUVECs. Principal components analysis (PCA) revealed the clear separation of the CT, AGE and calycosin groups, and there was tight clustering within each group. The calycosin group was closer to the CT than the AGE group, suggesting the partial restoration of endothelial metabolism (Fig. 3A). Using a fold-difference threshold of 1.3 and P<0.05, 126 metabolites were identified that were differentially regulated (77 upregulated and 49 downregulated) in the AGE vs. the CT group (Fig. 3B), 123 (51 upregulated and 72 downregulated) in the calycosin vs. the AGE group (Fig. 3C), and 91 (53 upregulated and 38 downregulated) in the calycosin vs. the CT group (Fig. 3D).

KEGG enrichment analysis revealed alterations in pathways related to energy and lipid metabolism, amino acid and cofactor biosynthesis and cellular signaling. To identify potentially reversible metabolic changes, a comparison was made between the pathways that were enriched in metabolites and upregulated in the AGE vs. the CT group and less enriched in the calycosin vs. the AGE group. A total of four metabolites (malonic acid, 3-hydroxyanthranilic acid, 2-arachidonoylglycerol and palmitic acid) were associated with nine overlapping pathways (pyrimidine metabolism, fatty acid biosynthesis, fatty acid metabolism, tryptophan metabolism, β-alanine metabolism, thermogenesis, retrograde endocannabinoid

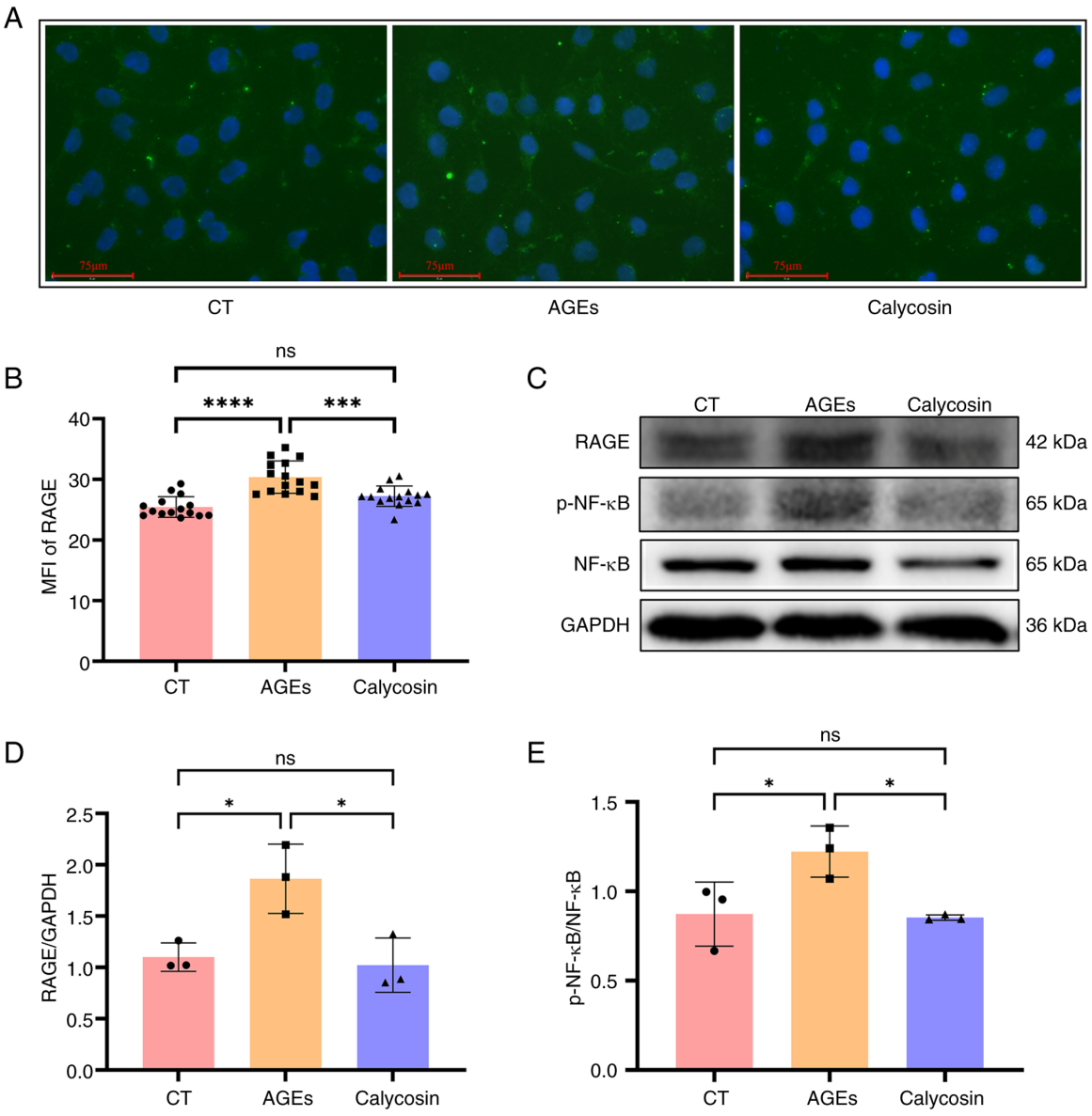


Figure 2. Calycosin attenuates RAGE and NF-κB phosphorylation in human umbilical vein endothelial cells induced by AGEs. (A and B) RAGE immunofluorescence staining and quantification of mean fluorescence intensity. (C-E) Representative western blots and quantification of RAGE and p-NF-κB/NF-κB (n=3). AGEs, advanced glycation end-products; RAGE, receptor for advanced glycation end-products; CT, normal culture medium; p-, phosphorylated; ns, not significant; *P<0.05; ***P<0.001; ****P<0.0001.

signaling, neuroactive ligand-receptor interaction and cofactor biosynthesis) (Fig. 4A and B). Metabolites that were downregulated in the AGE vs. the CT group were markedly enriched in carbon metabolism (Fig. 4C) and additional comparisons revealed distinct pathway alterations (Fig. 4D and E). Hierarchical clustering demonstrated that calycosin shifted the AGE-associated metabolic pattern toward that of the control state (Fig. 4F). These findings suggest that calycosin modulates multiple metabolic pathways that are involved in AGE-induced endothelial injury.

Calycosin ameliorates the abnormal vascular remodeling present in diabetic mice. The histological examination of thoracic aortas from the mouse groups was performed to evaluate the vascular protective effects of calycosin *in vivo*. H&E staining revealed that the diabetic mice had thicker walls than the controls (P<0.001) and that this defect was significantly less marked in the calycosin-treated mice (P<0.01; Fig. 5A). Masson and Sirius red staining demonstrated greater collagen deposition in the tunica media and adventitia of the diabetic mice, and that calycosin significantly reduced this collagen accumulation (P<0.05; Fig. 5B and C). The immunohistochemical analysis revealed that there was greater vascular NF-κB immunoreactivity in the diabetic mice (P<0.05) and that this was significantly reduced by treatment with calycosin (P<0.01; Fig. 5D). These findings indicate that calycosin attenuates diabetes-associated vascular remodeling, fibrosis and inflammation.

Calycosin improves the vascular function and reduces the systemic glycation burden of diabetic mice. The extent of Evans blue extravasation was assessed to evaluate the vascular permeability of the diabetic mice. The diabetic mice exhibited greater Evans blue staining in their vascular wall (Fig. 6A)

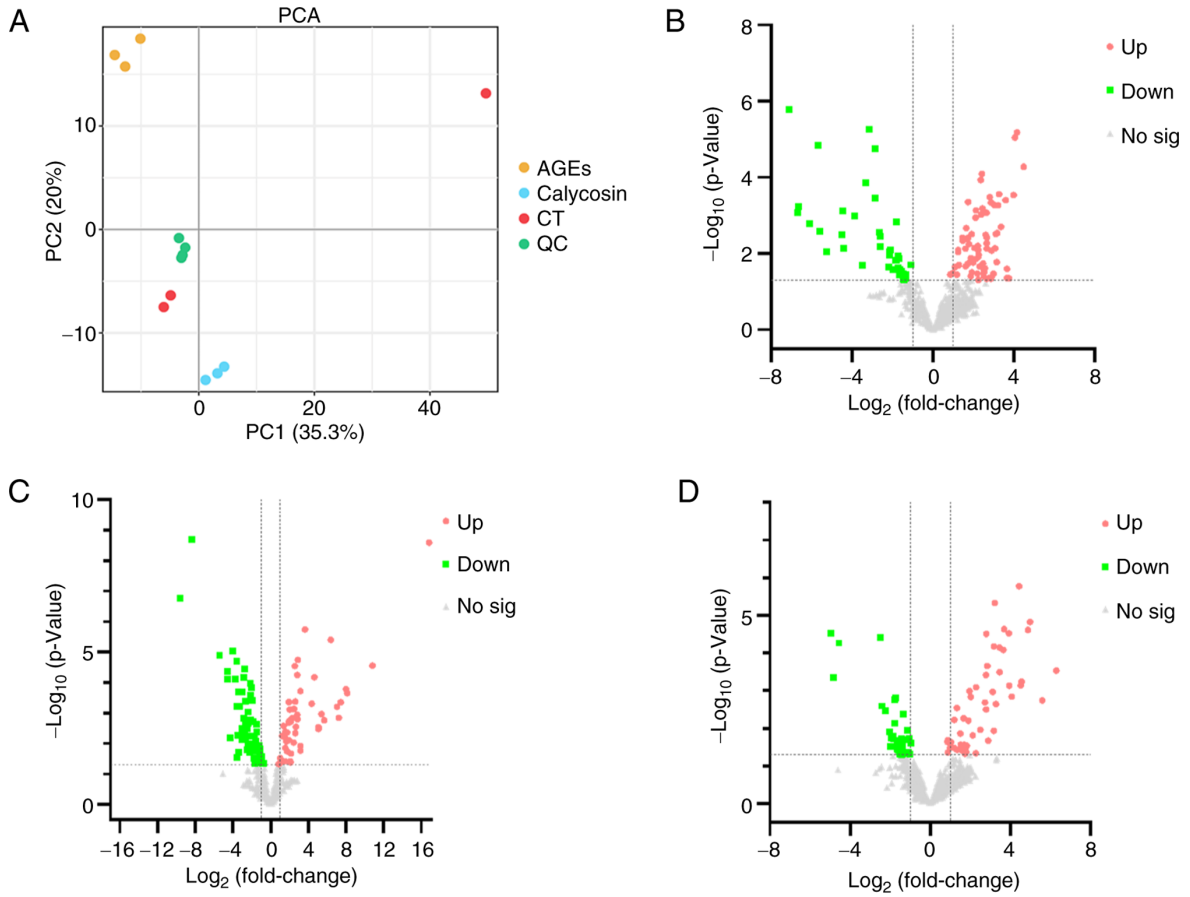


Figure 3. Calycosin partially restores AGE-associated endothelial metabolic profiles. (A) PCA of 725 metabolites identified by LC-MS/MS in the CT, AGE, calycosin and QC groups. (B-D) Volcano plots comparing (B) AGEs vs. CT, (C) calycosin vs. AGEs, and (D) calycosin vs. CT. Red and green indicate upregulated and downregulated metabolites, respectively. AGEs, advanced glycation end-products; PCA, principal components analysis; CT, normal culture medium; QC, quality control; Up, upregulation; down, downregulation.

and a significantly higher mean fluorescence intensity (MFI; P<0.01) than the control mice. However, treatment with calycosin markedly reduced the extravasation of the dye and the MFI (P<0.001; Fig. 6B), suggesting that it improved the integrity of the vascular barrier. ACh-induced vasorelaxation was evaluated using an *ex vivo* aortic ring assay, and rings from all groups exhibited concentration-dependent relaxation in response to ACh. The diabetic mice exhibited impaired ACh-induced relaxation compared with the controls, whereas treatment with calycosin ameliorated this response (Fig. 6C). These findings are consistent with improved vascular relaxation following calycosin treatment.

To assess systemic glycation, the present study measured the plasma AGE-associated fluorescence. The fluorescence intensity was significantly higher in the diabetic mice than in controls (P<0.05); however, treatment with calycosin significantly attenuated this increase (P<0.05; Fig. 6D), suggesting that it reduced glycation. The non-enzymatic glycation of plasma albumin was further analyzed using nanoLC-MS/MS, and of the 28 identified glycation sites, 22 lysine residues (K44, K57, K75, K97, K212, K257, K286, K305, K310, K341, K347, K383, K413, K421, K438, K460, K499, K524, K527, K549, K569 and K584) exhibited significantly greater glycation in the diabetic mice than in the controls. Treatment with calycosin reduced the relative glycation at these sites toward that of the control mice (Fig. 7). The remaining six sites (K65, K88, K267, K543, K588 and R141) exhibited non-significant downward trends following treatment. These findings suggest that calycosin treatment reduces the glycation of plasma albumin in diabetic mice.

Calycosin ameliorates the hyperglycemia and glucose intolerance of diabetic mice. Calycosin improved metabolic parameters in diabetic mice. Body weight gain was impaired in the DM group, whereas body weight initially decreased slightly and then stabilized in the calycosin-treated group (Fig. 8A). In addition, the higher food and water intakes of the diabetic mice were attenuated by treatment with calycosin (Fig. 8B and C). The blood glucose concentrations of the DM group were high (20-28 mmol/l); however, calycosin reduced these from day 4, and they were ~10 mmol/l after day 12 (Fig. 8D). Both groups of diabetic mice exhibited impaired glucose tolerance prior to treatment (Fig. 8E); however, calycosin significantly improved the glucose tolerance of the mice (P<0.01; Fig. 8F). These findings indicate that calycosin alleviates the hyperglycemia and improves the glucose homeostasis of diabetic mice.

AGE/RAGE-associated inflammatory signaling is reduced by calycosin. To further explore the molecular changes associated with the protective effects of calycosin, the unbiased proteomic profiling of AGE-treated HUVECs was performed.

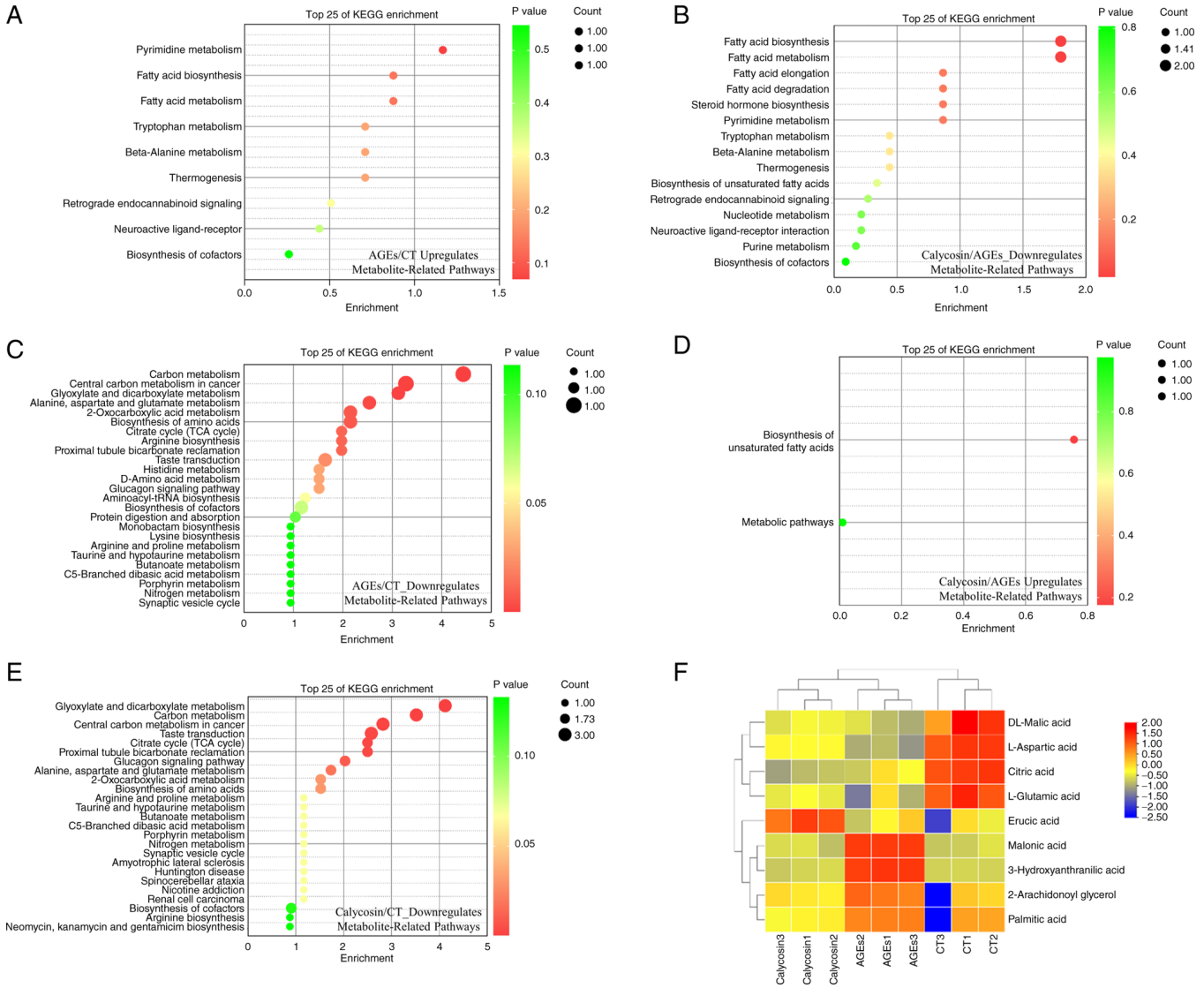


Figure 4. Calycosin modulates AGEs-associated endothelial metabolic remodeling. (A-E) KEGG pathway enrichment analysis of upregulated metabolites in (A) AGEs vs. CT, (B) downregulated metabolites in calycosin vs. AGEs, (C) downregulated metabolites in AGEs vs. CT, (D) upregulated metabolites in calycosin vs. AGEs, and (E) downregulated metabolites in calycosin vs. CT. (F) Heatmap of metabolite peak areas across experimental groups. AGEs, advanced glycation end-products; CT, normal culture medium.

KEGG enrichment analysis revealed the significant enrichment of the AGE/RAGE and NF-κB signaling pathways. Among the differentially expressed proteins, exposure to AGEs increased the abundances of transcription factor p65 (RELA) and urokinase-type plasminogen activator (PLAU), both of which were significantly reduced by calycosin treatment ($P<0.05$). Additionally, calycosin significantly reduced the abundance of protein diaphanous homolog 1 (DIAPH1), a cytosolic adaptor involved in RAGE signaling, vs. the AGE group ($P<0.05$; Fig. 9). These findings suggest that calycosin modulates RAGE-associated proinflammatory signaling, although the roles of DIAPH1, RELA and PLAU as specific molecular components require further functional validation.

Discussion

Diabetic vascular injury is driven by a complex interplay of chronic hyperglycemia, non-enzymatic glycation, endothelial inflammation, oxidative stress, metabolic dysfunction and vascular remodeling. The present study used AGE-treated HUVECs and mice with high-fat diet/STZ-induced diabetes to investigate the vascular protective effects of calycosin. Calycosin attenuated AGE-induced endothelial injury and metabolic dysregulation, and suppressed RAGE/NF-κB signaling. Consistent with this, it also reduced systemic glycation and ameliorated the abnormalities in vascular structure, endothelial barrier integrity and vasodilatory function in diabetic mice.

AGEs are critical mediators of diabetes-associated vascular injury and have been implicated in endothelial dysfunction, inflammation, and impaired vascular repair (21). In the present study, exposure to AGEs reduced the viability, increased the apoptosis, altered the morphology and impaired NO release by HUVECs. Calycosin improved the viability of the cells, increased NO release and reduced AGE-induced apoptosis, suggesting that it can help preserve endothelial homeostasis in the presence of glycation-related stress. These findings are consistent with the cytoprotective and anti-inflammatory

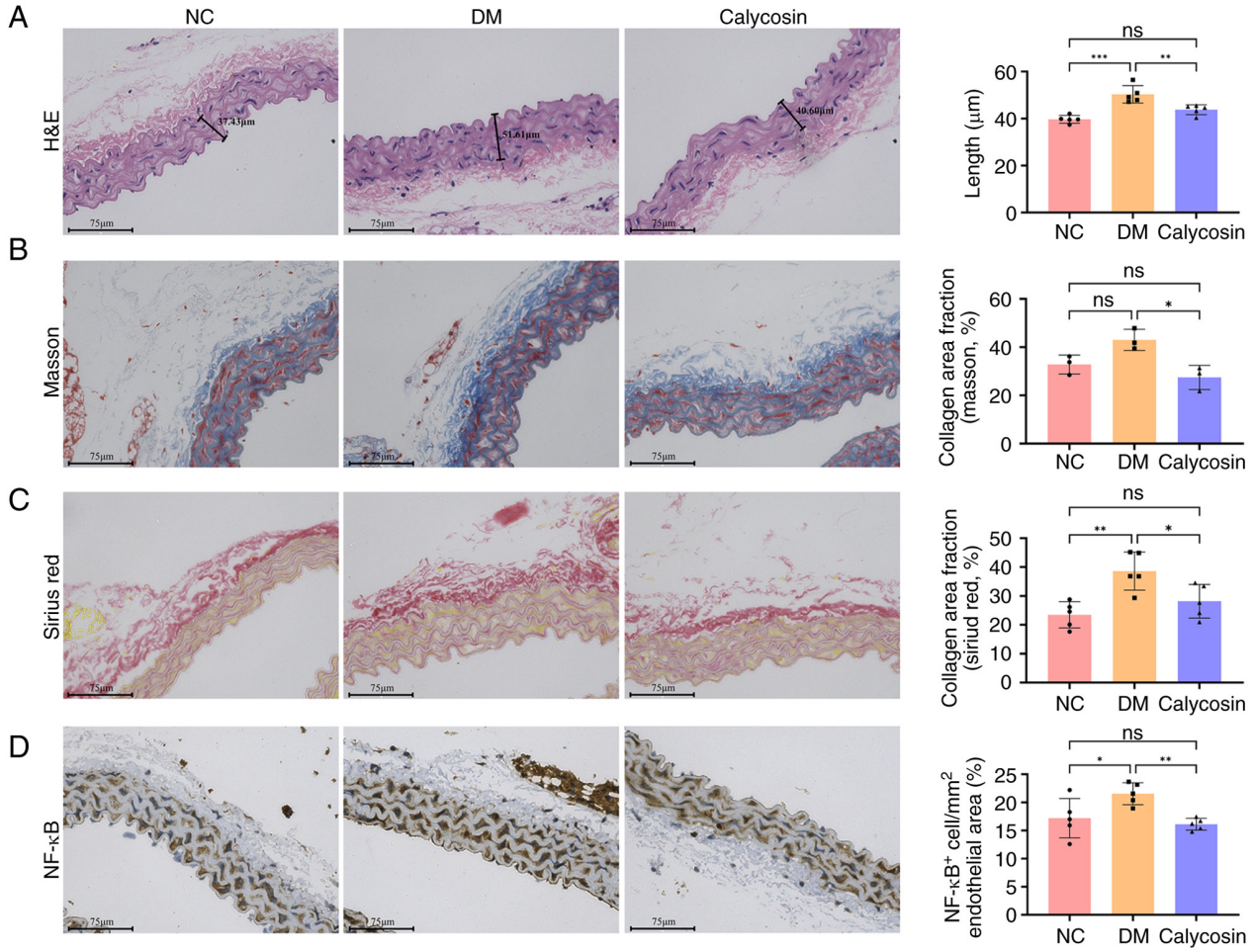


Figure 5. Calycosin attenuates thoracic aortic remodeling and NF-κB immunoreactivity in diabetic mice. (A) Representative H&E staining of thoracic aortic sections and quantification of vascular wall thickness (n=5). (B) Representative Masson's staining and quantification of aortic collagen deposition (n=3). (C) Representative Sirius red staining and quantification of aortic collagen deposition (n=5). (D) Representative immunohistochemical staining of NF-κB and quantification of the NF-κB-positive area ratio (n=5). H&E, hematoxylin and eosin; NC, normal control group; DM, type 2 diabetes group; ns, not significant; *P<0.05; **P<0.01; ***P<0.001.

properties of calycosin and related flavonoids that have previously been reported (22-26).

The AGE/RAGE axis is a key upstream mediator of the effects of glycation stress on endothelial inflammation. The binding of AGEs to RAGE increases oxidative stress and activates proinflammatory signaling pathways, including those involving NF-κB, thereby aggravating endothelial injury (27,28). In the present study, exposure to AGEs increased the RAGE immunofluorescence intensity, RAGE protein expression and NF-κB phosphorylation in HUVECs, and calycosin attenuated these changes. Previous research has demonstrated the involvement of AGE/RAGE signaling in the activation of NF-κB and endothelial injury in diabetes (29). To further evaluate the role of RAGE, RAGE was pharmacologically inhibited using FPS-ZM1. FPS-ZM1 pre-treatment significantly reduced NF-κB phosphorylation in AGE-treated HUVECs, supporting the involvement of RAGE in AGE-induced pro-inflammatory signaling. These findings, together with the identified effects of calycosin on RAGE expression and NF-κB signaling, suggest that the modulation of RAGE-associated proinflammatory signaling may contribute to its endothelial protective effects. Consistent with this, calycosin reduced the vascular NF-κB immunoreactivity of the diabetic mice.

Endothelial metabolic reprogramming is increasingly recognized to be a contributor to vascular dysfunction in diabetes (30). Untargeted metabolomics revealed substantial metabolic effects of AGE exposure, and the calycosin-treated HUVEC profile was shifted toward that of control cells. The altered sets of metabolites were associated with pathways involved in fatty acid, pyrimidine, tryptophan, and β-alanine metabolism, as well as endocannabinoid-related signaling and cofactor biosynthesis. Representative metabolites included malonic acid, palmitic acid, 3-hydroxyanthranilic acid, and 2-arachidonoylglycerol, each of which may be involved in endothelial metabolism (31-34). These findings suggest that calycosin may modulate interconnected endothelial metabolic networks, rather than a single metabolite.

The *in vivo* findings are also consistent with calycosin having vascular protective effects. The diabetic mice exhibited greater plasma AGE-associated fluorescence and high levels of glycation at multiple albumin residues, and calycosin treatment ameliorated these abnormalities, suggesting a reduction in systemic glycation. The concurrent improvement in glycemic control may also have contributed to the identified reduction in glycation. Histological analyses revealed vascular wall thickening and greater collagen deposition in the diabetic mice,

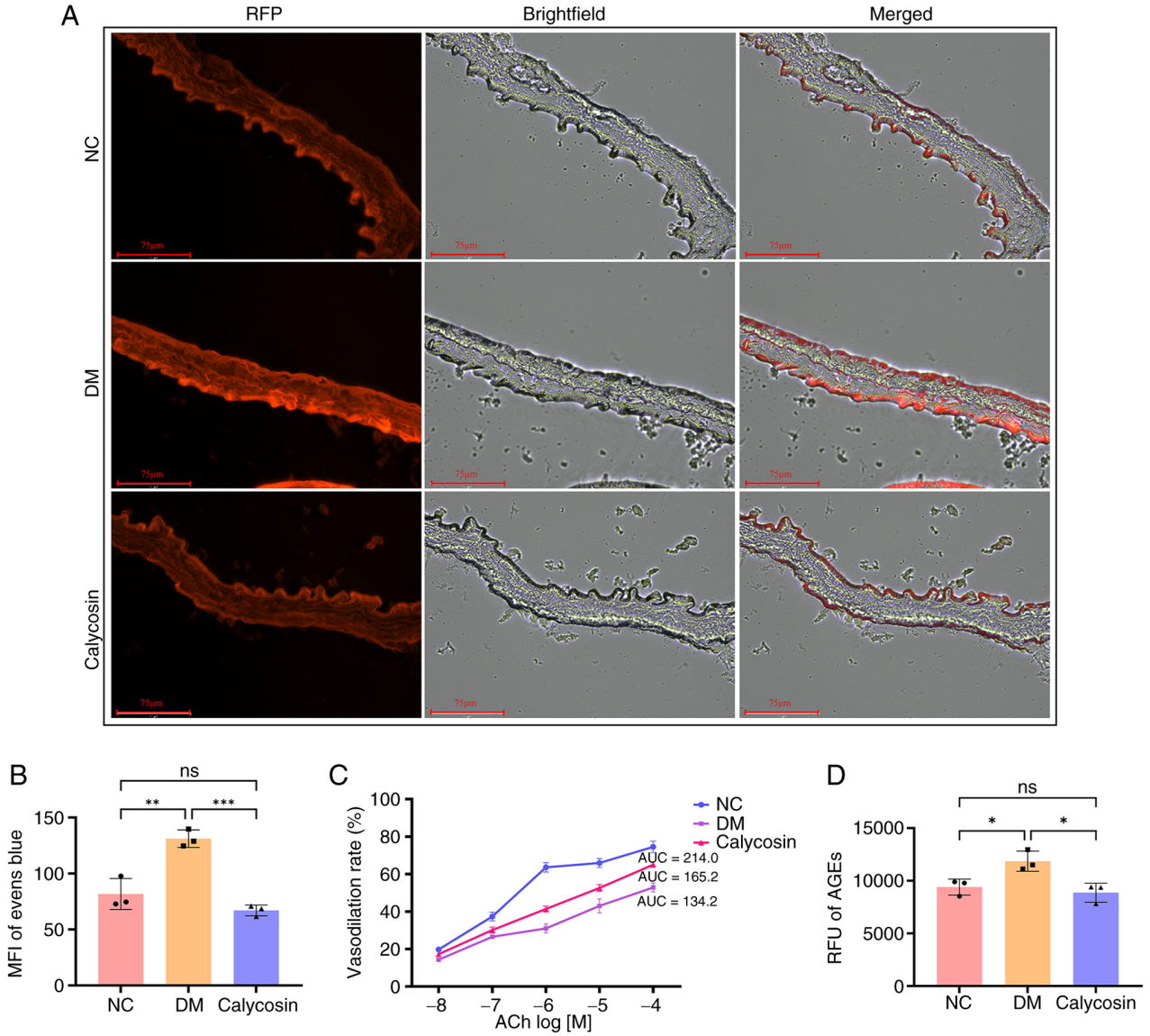


Figure 6. Calycosin improves vascular permeability and vasodilation in diabetic mice. (A) Representative images of Evans blue extravasation in thoracic aortas. Red fluorescence indicates the extent and distribution of dye leakage into the vascular wall; (B) quantitative analysis of MFI for Evans blue extravasation (n=3); (C) ACh-induced vasorelaxation (n=3); (D) plasma AGEs fluorescence levels following treatment of diabetic mice with calycosin (n=3). Data in panel C were analyzed using two-way repeated-measures ANOVA followed by Sidak post hoc tests. MFI, mean fluorescence intensity; ACh, acetylcholine; NC, normal control group; DM, type 2 diabetes group; RFP, red fluorescent protein channel; RFU, relative fluorescence units; ns, not significant; *P<0.05; **P<0.01; ***P<0.001.

and both of these abnormalities were ameliorated by calycosin treatment. These pathological changes are closely associated with the arterial stiffness and poor vascular compliance that characterize diabetes (35,36). AGEs promote cross-linking of the extracellular matrix, and RAGE-associated proinflammatory signaling may contribute to profibrotic responses and collagen deposition (37,38). Consistent with these mechanisms, calycosin reduced vascular NF-κB immunoreactivity and collagen accumulation, consistent with anti-inflammatory and anti-remodeling effects in vessels.

Diabetic endothelial injury compromises the integrity of the vascular barrier and endothelium-dependent vasodilation (39,40). In the present study, calycosin reduced Evans blue extravasation in the thoracic aorta and improved ACh-induced relaxation in aortic rings from diabetic mice, supporting beneficial effects on vascular barrier integrity and vascular function. Given the important contribution of endothelial NO signaling to ACh-induced vasodilation (41), these findings are consistent with the greater NO release identified in calycosin-treated HUVECs. These results further support the vascular protective effects of calycosin in diabetes.

Unbiased proteomics profiling revealed enrichment of the AGE/RAGE and NF-κB signaling pathways following calycosin treatment in AGE-treated HUVECs. Specifically, calycosin reduced the abundances of DIAPH1, RELA (p65) and PLAU. DIAPH1 is a cytosolic adaptor that is implicated in RAGE-mediated signaling (42), RELA is a component of the NF-κB transcriptional complex, and PLAU has been shown to be associated with NF-κB-related responses in other experimental contexts (43). Taken together with the identified reductions in RAGE expression and NF-κB phosphorylation, these proteomic findings provide further evidence to support the modulation of RAGE-associated proinflammatory signaling by calycosin.

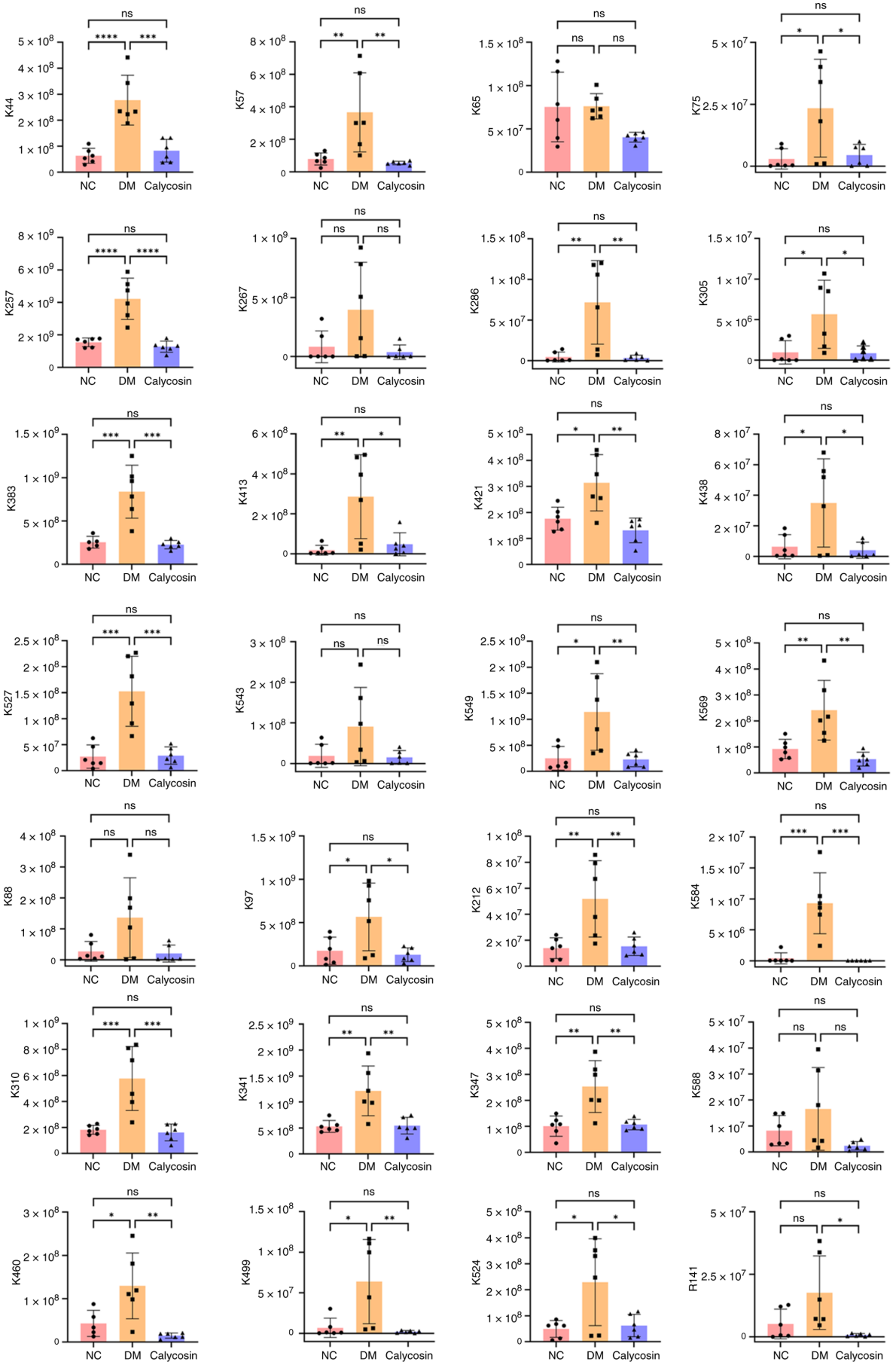


Figure 7. Calycosin reduces non-enzymatic glycation of plasma albumin in diabetic mice. Relative peak areas of glycation-modified peptides corresponding to 28 identified sites in mouse plasma albumin (n=6 per group). NC, normal control group; DM, type 2 diabetes group; ns, not significant; *P<0.05; **P<0.01; ***P<0.001; ****P<0.0001.

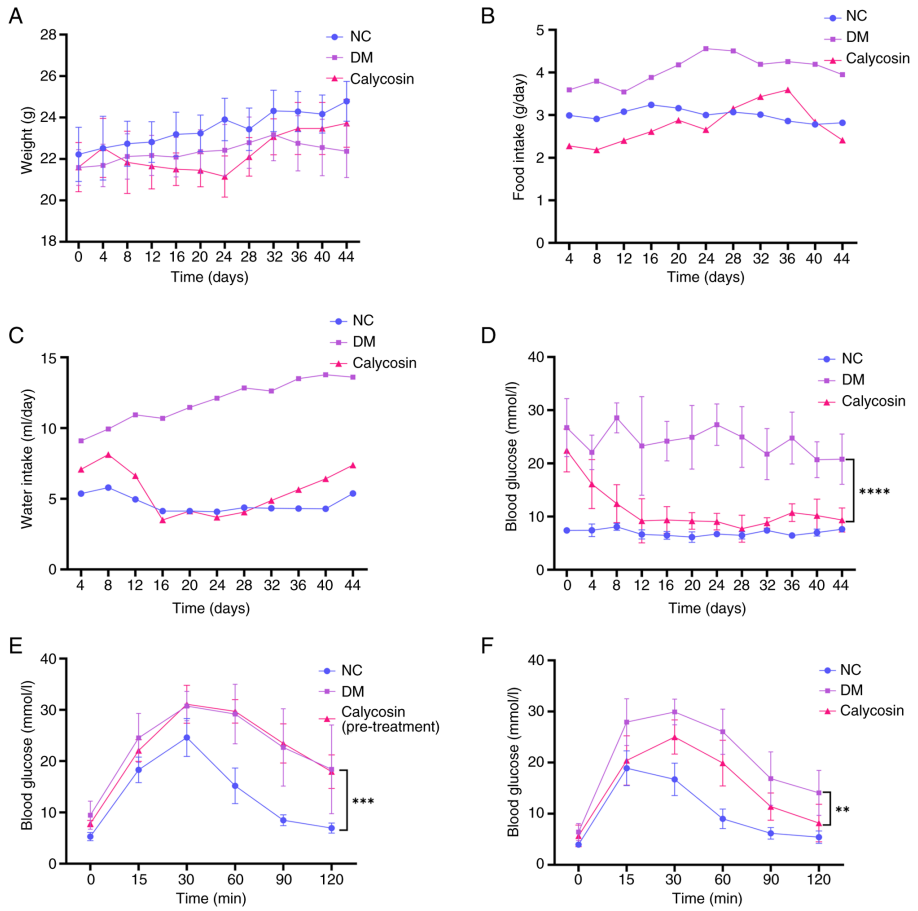


Figure 8. Effects of calycosin on physiological status and glucose in diabetic mice. (A) Body weight; (B) food intake; (C) water intake; (D) blood glucose levels; (E) OGTT prior to treatment; (F) OGTT following treatment (n=6/group for body weight, blood glucose and OGTT). Data were analyzed using two-way repeated-measures ANOVA followed by Sidak post hoc tests. NC, normal control group; DM, type 2 diabetes group. **P<0.01; ***P<0.001; ****P<0.0001.

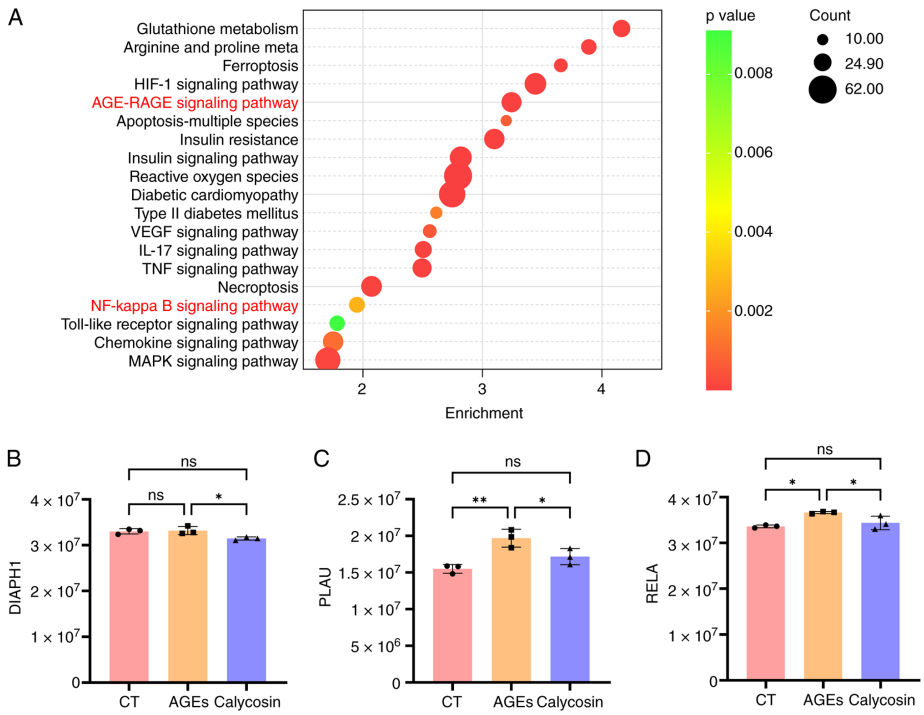


Figure 9. Proteomics analysis reveals alterations in AGE-RAGE and NF-κB signaling in human umbilical vein endothelial cells. (A) KEGG pathway enrichment analysis of differentially expressed proteins, with AGE–RAGE and NF-κB signaling pathways highlighted in red. (B-D) Quantification of (B) DIAPH1, (C) PLAU, and (D) RELA protein abundance based on mass spectrometry peak areas. AGEs, advanced glycation end-products; RAGE, receptor for advanced glycation end-products; DIAPH1, protein diaphanous homolog 1; PLAU, urokinase-type plasminogen activator; RELA, transcription factor p65; CT, normal culture medium; ns, not significant; *P<0.05; **P<0.01.

The findings of the present study suggest a working model in which glycation-associated inflammatory activation, endothelial metabolic disturbance, and impaired vascular function coexist in diabetes-related vascular injury. Calycosin attenuated these processes at several levels, as shown by less glycation of circulating proteins, altered RAGE/NF-κB-associated signaling, partial restoration of the endothelial metabolic profile, and improvements in vascular structure and function. These findings provide a mechanistic framework for further investigation of calycosin as a potential therapy for the vascular complications of diabetes.

Several limitations of the present study should be acknowledged. First, although the pharmacological inhibition of RAGE using FPS-ZM1 supports its involvement in AGE-induced NF-κB activation, it remains unclear whether RAGE is required for calycosin-mediated protection or whether calycosin directly interacts with RAGE. Second, because calycosin also improved glycemic control, the observed reduction in glycation may partly reflect lower blood glucose concentrations. Therefore, potential direct effects on AGE formation, precursor generation, and clearance require further investigation. Third, the metabolomic findings and the functional roles of proteins such as DIAPH1 and PLAU require further validation. Fourth, a full sodium nitroprusside concentration–response analysis was not performed; therefore, differences in vascular smooth muscle responsiveness cannot be excluded. Further studies are warranted to clarify the molecular mechanisms underlying the vascular protective effects of calycosin.

In conclusion, the present study demonstrates that calycosin attenuates diabetes-related endothelial and vascular injury, probably through effects including a reduction in glycation, the attenuation of inflammatory signaling, and the modulation of endothelial metabolic remodeling. In AGE-treated HUVECs, calycosin improved endothelial viability, reduced apoptosis, increased NO release, reduced RAGE expression and NF-κB phosphorylation, and shifted the AGE-associated metabolic profile toward that of the control cells. In diabetic mice, calycosin reduced systemic glycation, alleviated vascular inflammation and remodeling, preserved vascular barrier integrity, and improved ACh-induced vasorelaxation. Although further studies are required to confirm causal links and explore the translational significance of the present findings, they are consistent with calycosin being a potential therapy for the vascular complications of diabetes.

Acknowledgements

The authors would like to thank the staff of the Clinical Research Center, Affiliated Hospital of Shandong Second Medical University (Shandong, China), for their technical assistance with laboratory experiments and sample processing during the study.

Funding

The present study was supported by the Shandong Provincial Natural Science Foundation (grant nos. ZR2022QH013 and ZR2021QD132), the Shandong TCM Reform Demonstration Zone Science and Technology Co-construction Project (grant no. GZY-KJS-SD-2026-094), the Shandong Medical and Health Science and Technology Project (grant no. 202503061232), and the Taishan Scholars Project of Shandong Province (grant no. tsqn202211365).

Availability of data and materials

The data generated in the present study may be requested from the corresponding author. The metabolomics and proteomics datasets are available in OMIX (OMIX016659; https://ngdc.cncb.ac.cn/omix/release/OMIX016659) and iProX (IPX0020889000; https://www.iprox.cn/page/project.html?id=IPX0020889000), respectively.

Authors' contributions

JS and HT were involved in the conceptualization of the study, and were involved in the study methodology, data curation, and in the writing and preparation of the original draft of the manuscript. JC, HQ and XS were involved in the conceptualization of the study, in study supervision, and in the writing, reviewing and editing of the manuscript. WQ, YW, WZ, CK and YM were involved in data curation and investigation. HQ and XS confirm the authenticity of all the raw data. All authors have read and approved the final manuscript.

Ethics approval and consent to participate

All animal procedures were approved by the Institutional Animal Care and Use Committee of Shandong Second Medical University (2024SDL751) and were conducted in accordance with ARRIVE guidelines.

Patient consent for publication

Not applicable.

Competing interests

The authors declare that they have no competing interests.

References

1. Genitsaridi I, Salpea P, Salim A, Sajjadi SF, Tomic D, James S, Thirunavukkarasu S, Issaka A, Chen L, Basit A, *et al*: 11th edition of the IDF diabetes atlas: Global, regional, and national diabetes prevalence estimates for 2024 and projections for 2050. Lancet Diabetes Endocrinol 14: 149-156, 2026.
2. Ling W, Huang Y, Huang Y, Fan R, Sui Y and Zhao H: Global trend of diabetes mortality attributed to vascular complications, 2000-2016. Cardiovasc Diabetol 19: 182, 2020.
3. Shen C, Lu C, Wu C, Li K, Kuo Y, Hsieh S and Yu C: The development of maillard reaction, and advanced glycation end product (AGE)-receptor for AGE (RAGE) signaling inhibitors as novel therapeutic strategies for patients with AGE-related diseases. Molecules 25: 5591, 2020.
4. Salemkour Y and Lenoir O: Endothelial autophagy dysregulation in diabetes. Cells 12: 947, 2023.
5. Brahma S, Goyal AK, Dhamodhar P, Kumari MR, Jayashree S, Usha T and Middha SK: Can polyherbal medicine be used for the treatment of diabetes?-A review of historical classics, research evidence and current prevention programs. Curr Diabetes Rev 20: e140323214600, 2024.
6. Cheng X, Liu N, Liu H, Huang N, Sun X and Zhang G: Bioinformatic and biochemical findings disclosed anti-hepatic steatosis mechanism of calycosin. Bioorg Chem 100: 103914, 2020.

7. Deng M, Chen H, Long J, Song J, Xie L and Li X: Calycosin: A review of its pharmacological effects and application prospects. Expert Rev Anti Infect Ther 19: 911-925, 2021.
8. Qu N, Qu J, Huang N, Zhang K, Ye T, Shi J, Chen B, Kan C, Zhang J, Han F, *et al*: Calycosin induces autophagy and apoptosis via Sestrin2/AMPK/mTOR in human papillary thyroid cancer cells. Front Pharmacol 13: 1056687, 2022.
9. Ren F, Ma Y, Zhang K, Luo Y, Pan R, Zhang J, Kan C, Hou N, Han F and Sun X: Exploring the multi-targeting phytoestrogen potential of Calycosin for cancer treatment: A review. Medicine (Baltimore) 103: e38023, 2024.
10. An F, Zhao R, Xuan X, Xuan T, Zhang G and Wei C: Calycosin ameliorates advanced glycation end product-induced neurodegenerative changes in cellular and rat models of diabetes-related Alzheimer's disease. Chem Biol Interact 368: 110206, 2022.
11. Elsherbiny NM, Said E, Atef H and Zaitone SA: Renoprotective effect of calycosin in high fat diet-fed/STZ injected rats: Effect on IL-33/ST2 signaling, oxidative stress and fibrosis suppression. Chem Biol Interact 315: 108897, 2020.
12. Hu R, Wang M, Liu L, You H, Wu X, Liu Y, Wang Y, Lu L, Xiao W and Wei L: Calycosin inhibited autophagy and oxidative stress in chronic kidney disease skeletal muscle atrophy by regulating AMPK/SKP2/CARM1 signalling pathway. J Cell Mol Med 24: 11084-11099, 2020.
13. Song L, Li X, Bai XX, Gao J and Wang CY: Calycosin improves cognitive function in a transgenic mouse model of Alzheimer's disease by activating the protein kinase C pathway. Neural Regen Res 12: 1870-1876, 2017.
14. Wang X and Zhao L: Calycosin ameliorates diabetes-induced cognitive impairments in rats by reducing oxidative stress via the PI3K/Akt/GSK-3β signaling pathway. Biochem Biophys Res Commun 473: 428-434, 2016.
15. Xu Y, Feng L, Wang S, Zhu Q, Lin J, Lou C, Xiang P, He B, Zheng Z, Tang D and Zuo G: Phytoestrogen calycosin-7-O-β-D-glucopyranoside ameliorates advanced glycation end products-induced HUVEC damage. J Cell Biochem 112: 2953-2965, 2011.
16. Li Y, Duan B, Li Y, Yu S and Wang Y: The isoflavonoid calycosin inhibits inflammation and enhances beta cell function in gestational diabetes mellitus by suppressing RNF38 expression. Immunopharmacol Immunotoxicol 42: 366-372, 2020.
17. Zhang Y, Tan R, Zhang X, Yu Y and Yu C: Calycosin ameliorates diabetes-induced renal inflammation via the NF-κB pathway in vitro and in vivo. Med Sci Monit 25: 1671-1678, 2019.
18. Gilbert ER, Fu Z and Liu D: Development of a nongenetic mouse model of type 2 diabetes. Exp Diabetes Res 2011: 416254, 2011.
19. Heinen A, Spychala A, Ballmann L, Gödecke S, Faradj Z, Bresch F, Krüger M, Bottermann K, Zabri H, Fischer J, *et al*: Combined high-fat, high-sucrose diet and streptozotocin treatment induces cardiometabolic heart failure with preserved ejection fraction in mice. Am J Physiol Heart Circ Physiol 330: H1375-H1390, 2026.
20. Zhang L, Kan C, Shi J, Qiu H, Zhang J, Ding W, Xu L, Zhang K, Guo Z, Hou N, *et al*: Sestrin2 knockout exacerbates high-fat diet induced metabolic disorders and complications in female mice. Nutr Metab (Lond) 21: 60, 2024.
21. Takeuchi M, Takino J and Yamagishi S: Involvement of the toxic AGEs (TAGE)-RAGE system in the pathogenesis of diabetic vascular complications: A novel therapeutic strategy. Curr Drug Targets 11: 1468-1482, 2010.
22. Adu MD, Bondonno CP, Parmenter BH, Sim M, Davey RJ, Murray K, Radavelli-Bagatini S, Magliano DJ, Daly RM, Shaw JE, *et al*: Association between non-tea flavonoid intake and risk of type 2 diabetes: The Australian diabetes, obesity and lifestyle study. Food Funct 13: 4459-4468, 2022.
23. Gong G, Zheng Y, Yang Y, Sui Y and Wen Z: Pharmaceutical values of calycosin: One type of flavonoid isolated from Astragalus. Evid Based Complement Alternat Med 2021: 9952578, 2021.
24. Yosri H, El-Kashef DH, El-Sherbiny M, Said E and Salem HA: Calycosin modulates NLRP3 and TXNIP-mediated pyroptotic signaling and attenuates diabetic nephropathy progression in diabetic rats; an insight. Biomed Pharmacother 155: 113758, 2022.
25. Han F, Li K, Pan R, Xu W, Han X, Hou N and Sun X: Calycosin directly improves perivascular adipose tissue dysfunction by upregulating the adiponectin/AMPK/eNOS pathway in obese mice. Food Funct 9: 2409-2415, 2018.
26. Ma T, Zhang Z, Chen Y, Su H, Deng X, Liu X and Fan Y: Delivery of nitric oxide in the cardiovascular system: Implications for clinical diagnosis and therapy. Int J Mol Sci 22: 12166, 2021.
27. Pal R and Bhadada SK: AGEs accumulation with vascular complications, glycemic control and metabolic syndrome: A narrative review. Bone 176: 116884, 2023.
28. Venkatesan B, Valente AJ, Das NA, Carpenter AJ, Yoshida T, Delafontaine J, Siebenlist U and Chandrasekar B: CIKS (Act1 or TRAF3IP2) mediates high glucose-induced endothelial dysfunction. Cell Signal 25: 359-371, 2013.
29. Khalid M, Petroianu G and Adem A: Advanced glycation end products and diabetes mellitus: Mechanisms and perspectives. Biomolecules 12: 542, 2022.
30. Pan Y and Si J: Endothelial metabolic reprogramming links diabetes to atherosclerosis. Diabetes Metab Syndr Obes 19: 565805, 2026.
31. Garcia D and Shaw RJ: AMPK: Mechanisms of cellular energy sensing and restoration of metabolic balance. Mol Cell 66: 789-800, 2017.
32. Jung K, Clapper JR, Fu J, D'Agostino G, Guijarro A, Thongkham D, Avanesian A, Astarita G, DiPatrizio NV, Frontini A, *et al*: 2-Arachidonoylglycerol signaling in forebrain regulates systemic energy metabolism. Cell Metab 15: 299-310, 2012.
33. Pae H, Oh G, Lee B, Rim J, Kim Y and Chung H: 3-Hydroxyanthranilic acid, one of L-tryptophan metabolites, inhibits monocyte chemoattractant protein-1 secretion and vascular cell adhesion molecule-1 expression via heme oxygenase-1 induction in human umbilical vein endothelial cells. Atherosclerosis 187: 274-284, 2006.
34. Sivri D and Akdevelioğlu Y: Effect of fatty acids on glucose metabolism and type 2 diabetes. Nutr Rev 83: 897-907, 2025.
35. Stehouwer CDA, Henry RMA and Ferreira I: Arterial stiffness in diabetes and the metabolic syndrome: A pathway to cardiovascular disease. Diabetologia 51: 527-539, 2008.
36. Woodman RJ, Chew GT and Watts GF: Mechanisms, significance and treatment of vascular dysfunction in type 2 diabetes mellitus: Focus on lipid-regulating therapy. Drugs 65: 31-74, 2005.
37. Serban AI, Stanca L, Geicu OI, Munteanu MC and Dinischiotu A: RAGE and TGF-β1 cross-talk regulate extracellular matrix turnover and cytokine synthesis in AGEs exposed fibroblast cells. PLoS One 11: e0152376, 2016.
38. Vaez M, Asgari M, Hirvonen L, Bakir G, Khattignavong E, Ezzo M, Aguayo S, Schuh CM, Gough K and Bozec L: Modulation of the biophysical and biochemical properties of collagen by glycation for tissue engineering applications. Acta Biomater 155: 182-198, 2023.
39. Bahadoran Z, Mirmiran P, Kashfi K and Ghasemi A: Vascular nitric oxide resistance in type 2 diabetes. Cell Death Dis 14: 410, 2023.
40. Wang Y, Huang H, Shao F, Eshwaran R, Qin M, Karim N, Ren Y, Dobreva G, Hammes HP, Wieland T and Feng Y: Disrupting VE-cadherin Y685 phosphorylation inhibits development of experimental diabetic and prediabetic retinopathy. J Clin Invest 136: e195048, 2026.
41. Støen R, Lossius K and Karlsson JOG: Acetylcholine-induced vasodilation may depend entirely upon NO in the femoral artery of young piglets. Br J Pharmacol 138: 39-46, 2003.
42. Yepuri G, Hasan SN, Kumar V, Manigrasso MB, Theophall G, Shekhtman A, Schmidt AM and Ramasamy R: Mechanistic underpinnings of AGEs-RAGE via DIAPH1 in ischemic, diabetic, and failing hearts. Am J Physiol Heart Circ Physiol 328: H1026-H1037, 2025.
43. Zhou T, Sun J, Shi W, Zhou Y, Ding X, Cai X and Cai Y: Integrated transcriptomics and experimental validation reveal that ellagic acid alleviates fuchs endothelial corneal dystrophy via PLAU/NF-κB signaling. Invest Ophthalmol Vis Sci 67: 31, 2026.

Copyright © 2026 Shi et al. This work is licensed under a Creative Commons Attribution-NonCommercial-NoDerivatives 4.0 International (CC BY-NC-ND 4.0) License.